Version 2 Goddard Satellite-Based Surface Turbulent Fluxes (GSSTF2)

Shu-Hsien Chou
Laboratory for Atmospheres
NASA Goddard Space Flight Center
Greenbelt, Maryland

Eric Nelkin
Science Systems & Applications, Inc.
Lanham, Maryland

Joe Ardizzone
Science Applications International Corporation
Laurel, Maryland

Robert M. Atlas
Laboratory for Atmospheres
NASA Goddard Space Flight Center
Greenbelt, Maryland

Chung-Lin Shie
UMBC/Goddard Earth and Sciences Technology Center
NASA Goddard Space Flight Center
Greenbelt, Maryland

Journal of Climate
October 22, 2002

Corresponding author: Dr. Shu-Hsien Chou, Code 912, Laboratory for Atmospheres, NASA Goddard Space Flight Center, Greenbelt, MD 20771.
E-mail: chou@agnes.gsfc.nasa.gov

1. Introduction

The earth climate is a coupled system involving ocean, land, and atmosphere. Information on the turbulent, radiative, and freshwater fluxes at the air-sea interface is essential in understanding the interaction between the atmosphere and oceans and in improving model simulations of climate variations. These fluxes are required for driving ocean models and validating coupled ocean-atmosphere global models. Surface measurements of these fluxes are scarce in both space and time. The Comprehensive Ocean-Atmosphere Data Set (COADS) has collected the most complete surface marine observations since 1854, mainly from merchant ships (Woodruff et al. 1993). However, the air-sea fluxes and input variables based on COADS have serious spatial and temporal sampling problems plus measurement uncertainty (e.g., da Silva et al. 1994; Josey et al. 1999; Wang and McPhaden 2001). Therefore, it is desirable that long-term global datasets of these fluxes be derived either from satellite observations or general circulation models (GCM). In recognition of the importance of these fluxes in climate studies, the World Climate Research Program (WCRP) Global Energy and Water Experiment (GEWEX) has established a Surface Radiation Budget (SRB) project and the GEWEX Global Precipitation Climatology Project (GPCP), with the primary objectives of deriving the global datasets of surface radiation and precipitation from satellite observations. In addition, an ocean surface turbulent flux project (SEAFLUX; Curry et al. 2002) has been established to conduct intercomparison studies of sea surface turbulent fluxes, flux models, and input variables used for the derivation of turbulent fluxes.

Several efforts are underway to prepare datasets of ocean surface turbulent fluxes from satellite observations using bulk flux models (Curry et al. 2002 and references within). The Special Sensor Microwave/Imager (SSM/I) on board a series of the Defense Meteorological Satellite Program (DMSP) spacecraft has provided global radiance measurements for sensing the atmosphere and the surface. A number of techniques have been developed to derive the turbulent fluxes using parameters such as the surface air humidity and winds inferred from the SSM/I radiances (e.g., Chou et al. 1997; Schulz et al. 1997; Curry et al. 1999; Kubota et al. 2002a; Curry et al. 2002).

Currently, there are several global datasets of ocean surface turbulent fluxes available, which are based on the SMM/I-retrieved surface air humidity and winds. The Hamburg Ocean Atmosphere Parameters and Fluxes from Satellite Data (HOAPS) has provided pentad and monthly turbulent heat fluxes over global oceans with 1° spatial resolution for the period July 1987–December 1998, based on the method of Schulz et al. (1997). The Goddard Satellite-based Surface Turbulent Fluxes (GSSTF) has two versions of global flux products derived from the SSM/I radiances. The version 1 (GSSTF1) has daily and monthly fields for July 1987–December 1994 with a spatial resolution of 2.0° x 2.5° lat–long (Chou et al. 1997, 2000). The version 2 (GSSTF2) has daily and monthly fields for July 1987–December 2000 with 1° resolution, based on the method of Chou et al. (1997) with some improvements (see the appendix). The Japanese Ocean Flux dataset with Use of Remote sensing Observations (J-OFURO) has provided monthly turbulent heat fluxes over global oceans with 1° resolution for 1991–95 (Kubota et al., 2002a). These four and other flux datasets have been distributed to the SEAFLUX web site for intercomparison studies. Both GSSTF1 and GSSTF2 are also available at http://daac.gsfc.nasa.gov/CAMPAIGN_DOCS/hydrology/hd_gsstf2.0.html.

The satellite retrieved air-sea fluxes and input variables are subject to retrieval errors. On the other hand, errors in the surface fluxes and input variables of GCMs can arise from the imperfect parameterization of physical processes, especially the boundary layer processes (e.g., Weller and Anderson 1996; Wang and McPhaden 2001). The scientists at the NOAA/Environmental Technology Laboratory (ETL) have conducted several field experiments to provide high quality data of surface meteorology and air-sea fluxes over the oceans using research ships (e.g., Fairall et al. 1996a, 1997). These data are very valuable for the validation of satellite retrievals and GCM products.

The purpose of this paper is to present an assessment of GSSTF2, which is one of the SEAFLUX activities. Section 2 describes the data sources used in this study. Section 3 discusses the methodology for the satellite retrieval of daily turbulent fluxes, as well as the collocation validation of daily input variables and turbulent fluxes of GSSTF2 against daily measurements of nine NOAA/ETL field experiments. Section 4 presents the spatial distributions of the GSSTF2

annual- and seasonal-mean turbulent fluxes and input variables averaged over 1988–2000. Section 5 compares zonal averages of latent heat fluxes and input variables over global oceans during 1992–93 for GSSTF1, GSSTF2, HOAPS, NCEP/NCAR reanalysis (Kalnay et al. 1996), and da Silva et al. (1994). Concluding remarks are given in section 6. The appendix briefly discusses the GSSTF2 bulk aerodynamic algorithm, as well as the validation against hourly flux measurements of ten experiments conducted by the NOAA/ETL research ships over the tropical and midlatitude oceans during 1991–99.

2. Data sources

Daily turbulent fluxes of momentum, moisture, and heat are derived from the version-4 SSM/I surface (10-m) wind speeds and total precipitable water of Wentz (1997), as well as the sea surface temperature (SST), 2-m air temperature and sea-level pressure of NCEP/NCAR reanalysis. The DMSP satellites pertinent to this study are F8, F10, F11, F13, and F14, which are polar orbiting with a period of ~102 min. Table 1 shows the approximate local times of equatorial crossing and data records for each of these satellites. Since January 1991, the earth system has been sensed by at least two SSM/Is with enhanced spatial and temporal coverage. Each satellite had a swath of 1394 km on the earth surface. The SSM/I-retrieved surface winds and water vapor amounts have an original spatial resolution of $(25\ \text{km})^2$. They are averaged to daily values over 1° x 1° lat–long regions using data from all available DMSP satellites.

To validate the bulk flux algorithm, surface turbulent fluxes, and input parameters of GSSTF2, hourly measurements of surface meteorology and turbulent fluxes of ten field experiments conducted by the NOAA/ETL research ships (Fairall et al. 1997) over the tropical and midlatitude oceans during 1991–99 are used. These ten experiments are the Atlantic Stratocumulus Transition Experiment (ASTEX), the Coupled Ocean-Atmosphere Response Experiment (COARE), the Fronts and Atlantic Storm Track Experiment (FASTEX), the Joint Air-Sea Monsoon Interaction Experiment (JASMINE), the Kwajalein Experiment (KWAJEX), the Nauru '99 (NAURU99), the San Clemente Ocean Probing Experiment (SCOPE), the Tropical Instability Wave Experiment (TIWE), the Pan-American Climate Study in the eastern Pacific during 1999 (PACSF99), and the buoy service in the North Pacific (MOORINGS). Periods and locations of these experiments are

listed in Table A1. These ten experiments provided hourly (50 min) covariance latent heat flux (LHF) and sensible heat flux (SHF) derived using the eddy correlation method. The experiments also provided hourly wind stresses computed using the inertial-dissipation (ID) method, which are more accurate than those derived using the eddy correlation method (Fairall et al. 1996a). To reduce the flow distortion effects, only the data with the relative wind direction within 30° of the bow are used, except for SCOPE (Yelland et al. 1998). For SCOPE, data with wind directions 60--100° relative to the bow are excluded. In addition, the latent heat fluxes and input variables of GSSTF1, HOAPS, NCEP/NCAR reanalysis, and da Silva et al. (1994) over global oceans for the period 1992–93 are used to compare with those of GSSTF2.

3. Methodology and validation for GSSTF2

a. Methodology for retrieving daily air-sea turbulent fluxes

Surface turbulent fluxes are derived from the SSM/I version-4 data of Wentz (1997) using a stability-dependent bulk aerodynamic algorithm given in the appendix. Input parameters are daily mean values of SST, saturation specific humidity at the sea surface (Q_S), wind speed (U_{10m}) and specific humidity 10 m above the surface (Q_{10m}), and air temperature 2 m above the surface (T_{2m}). It is noted that the reference height in the bulk scheme is set to 10 m for wind speed and humidity but is set to 2 m for temperature, for correctly calculating their gradients and stability (Chou et al. 1997). The 10-m wind speed and specific humidity are derived from radiances measured by the SSM/I. The 10-m specific humidity is derived from the water vapor amount in the entire atmospheric column taken from Wentz (1997) and the lowest 500-m layer above the surface using the method developed by Chou et al. (1995, 1997). The latter is retrieved from the SSM/I radiances using the method of Schulz et al. (1993). The SSM/I 10-m wind speeds of Wentz (1997) are used. The directions of wind stress are taken from those of the surface winds, which are derived from a blend of the SSM/I surface wind speeds (Wentz 1997), surface wind vectors from ships, buoys, and the NCEP/NCAR reanalysis following the method of Atlas et al. (1996).

The latent and sensible heat fluxes depend on the skin SST. The SST of the NCEP/NCAR reanalysis is derived by regressing the bulk SST against the satellite IR radiance measurements (Reynolds and Smith 1994). The daily mean bulk SST is generally warmer than the skin SST by

~0.2 °C with the difference depending on surface net heat flux and wind-induced oceanic mixing (Fairall et al. 1996b; Webster et al. 1996; Weller and Anderson 1996; Wick et al. 1996). The global distribution of skin SST for the period of interest is not currently available and is still under extensive study (Curry et al. 2002). Thus we use the bulk SST of the NCEP/NCAR reanalysis to compute heat fluxes.

The Q_S is determined from the daily mean SST and sea-level pressure of the NCEP/NCAR reanalysis. As discussed in the appendix, it is computed from the approximated formulation of the specific humidity to partially account for the cool skin effect. It also includes the 2% reduction in the saturation vapor pressure for saline water as compared to pure water (Fairall et al. 1996a; Zeng et al. 1998; Curry et al. 1999). To use a bulk aerodynamic scheme to derive surface sensible heat fluxes, the measurements of air temperatures in the atmospheric surface layer (with a depth of ~50–100 m) are required. However, they are not available from satellite measurements. Thus, the daily mean T_{2m} used for computing sensible heat flux is taken from that of the NCEP/NCAR reanalysis. Sea-air temperature difference is generally very small over the open ocean, except for the western Pacific warm pool and midlatitudes in the winter. Small errors in the SSTs and air temperatures could induce a relatively large error in the sea-air temperature difference if the errors are uncorrelated. The 2-m temperature of the NCEP/NCAR reanalysis is thermodynamically constrained to the SST.

b. Collocation validation for GSSTF2

Table 2 and Figs. 1 and 2 compare daily-mean GSSTF2 turbulent fluxes and input variables with those of ten field experiments conducted by the NOAA/ETL (Table A1) except for SCOPE. Note that there are no data for GSSTF2 to collocate with SCOPE as it is too close to the coastline. Therefore, only nine experiments are used in the collocation validation. The daily GSSTF2 wind speed, humidity, and temperature of the surface air are adjusted using the GSSTF2 bulk scheme to the measurement heights of the ships (~14–21 m) for proper validation. The GSSTF2 daily SST is compared with the bulk SST at the 5-cm depth measured by the ships. The comparison with five major tropical experiments with large samples (ASTEX, COARE, JASMINE, NAURU99, and KWAJEX) is also shown in Table 2 for reference.

Table 2 shows that the GSSTF2 surface air humidity has a positive bias of ~1 g kg^{-1} in the tropical oceans, especially when the humidity is >16 g kg^{-1} (Fig. 2b). However, the LHF has only a small negative bias of ~ –2.6 W m^{-2} in the tropical oceans. This is mainly due to the fact that, in the tropical oceans, the weak winds have a small positive bias of ~0.3 m s^{-1} and the GSSTF2 bulk flux scheme has a small positive bias of ~5 W m^{-2} for LHF (Tables 2 and A2). These two factors offset the underestimation of LHF due to a negative bias of sea-air humidity difference. On the other hand, the GSSTF2 SHF has a large positive bias of ~7 W m^{-2} in the tropical oceans. This is mainly due to the negative bias of surface air temperature of the NCEP/NCAR reanalysis, especially for T_a<26 °C (Fig. 2c), a fact that was also found by Smith et al. (2001), and Wang and McPhaden (2001).

Sources of retrieval-ship differences in daily turbulent fluxes and input parameters include the spatial-temporal mismatch between GSSTF2 and ships, as well as the errors in the input parameters and fluxes for both GSSTF2 and ship observations. The collocated daily GSSTF2 variables are computed from 2–3 satellite observations averaged over an 1° area that encloses the ship locations, while those of the ships are computed from at least two hourly measurements over a much smaller area. Assuming daily retrieval errors are independent, Table 2 shows the SD errors for the monthly-mean wind stress, LHF, and SHF to be 0.0136 (0.0035) N m^{-2}, 6.5 (5.4) W m^{-2}, and 1.8 (1.1) W m^{-2}, respectively, as inferred from the nine (five tropical) experiments. The SD errors for the monthly mean wind speed, humidity, and temperature of the surface air, and SST are 0.25 (0.20) m s^{-1}, 0.22 (0.20) g kg^{-1}, 0.15°C (0.14°C), and 0.09°C (0.05°C), respectively, as inferred from the nine (five tropical) experiments.

4. 1988–2000 annual- and seasonal-mean air-sea turbulent fluxes

a. Annual means

Figure 3 shows spatial distributions of the GSSTF2 annual-mean surface (10-m) wind speed, sea–air humidity difference (Q_S–Q_{10m}), and sea–air temperature difference (SST–T_{2m}) averaged over 1988–2000, respectively. Figure 4 shows spatial distributions of the GSSTF2 annual-mean wind stress, LHF, and SHF averaged over the same 13-yr period, respectively. Figures 3a and 4a show that the maximum annual mean wind speed and stress are located in the trade-wind belts (~8–9 m s^{-1}

^{1}, ~0.09–0.12 N m^{-2}) and extratropical storm-track regions (~8–11 m s^{-1}, ~0.09–0.2 N m^{-2}). The minimum annual-mean wind speed and stress (<~0.03 N m^{-2}) are located in the weak-wind (~4–6 m s^{-1}) areas of the intertropical convergence zone (ITCZ), South Pacific convergence zone (SPCZ), and tropical Indian Ocean, as well as the subtropical highs (~7 m s^{-1}). Figure 4b shows that the maximum LHF is located in the trade wind belts (~150–180 W m^{-2}) and in the western boundary current regions of Kuroshio and Gulf Stream (~150 W m^{-2}). This results from high winds (~8–9 m s^{-1}) coupling with large Q_S–Q_{10m} (~5–6 g kg^{-1}) in these areas as shown in Figs. 3a and 3b. The minimum LHF (<~60 W m^{-2}) is found in the eastern equatorial Pacific and Atlantic, due to upwelling-induced cold SSTs associated with weak winds, and in the high latitudes due to poleward decrease of SST. The SHF is generally very small (<~10–15 W m^{-2}) due to the smallness of SST–T_{2m} (<~1–1.5°C), except for slightly larger fluxes in the northwestern parts of the North Pacific and North Atlantic arising from cold air outbreaks (Figs. 3c and 4c).

The spatial distributions of the GSSTF2 annual-mean latent heat flux and relevant input parameters averaged over 1988–2000 (Figs. 3 and 4) are similar to those of GSSTF1, HOAPS, J–OFURO and NCEP/NCAR reanalysis (Kubota et al. 2002b). However, there are quantitative differences among various global flux datasets. The intercomparisons of LHF and input parameters are presented in section 5.

b. Seasonal means

The seasonal-mean wind stress and latent heat flux along with the relevant input parameters averaged over the four seasons of December, January, February (DJF), March, April, May (MAM), June, July, August (JJA), September, October, and November (SON) of 1988–2000 are discussed. Figures 5 and 6 show the spatial distributions of the GSSTF2 seasonal-mean 10-m wind speed and stress for the 1988–2000 four seasons, respectively. The maximum wind speed and stress are generally found in the trade-wind zones, the tropical Indian Ocean (associated with the southwest summer Monsoon circulation), the wintertime extratropical North Pacific and North Atlantic (associated with synoptic activities), and the Southern Hemisphere extratropical oceans. The wind speed and stress in the trade wind zones are larger in the Northern Hemisphere than in the Southern Hemisphere during DJF and MAM, and vice versa during the other two seasons, as a result of

seasonal variations of the Hadley circulation. The minimum wind speed and stress are generally found in the tropical Indian Ocean and SPCZ during DJF and MAM, near Indochina during JJA and SON, the ITCZ in the eastern equatorial Pacific and Atlantic, and the subtropical highs. The surface wind speed and stress fields, shown in Figs. 5 and 6, clearly demonstrate the seasonal variations of the atmospheric general circulation. The spatial distributions of seasonal-mean surface wind and stress are similar to those of GSSTF1 (Chou et al. 1997), Atlas et al. (1996), Esbensen et al. (1993), Chou et al. (1995), and Hellerman and Rosenstein (1983).

Figures 7 and 8 show spatial distributions of the GSSTF2 seasonal mean Q_S–Q_{10m} and LHF averaged over 1988-2000, respectively. The patterns of the seasonal-mean LHF follow more closely those of the surface wind speed in the tropical oceans, but more closely those of Q_S–Q_{10m} in the extratropical oceans and the equatorial eastern Pacific and Atlantic (Figs. 5, 7, and 8). All three variables are larger in the winter than in the summer hemisphere. The high LHF (~180–210 W m^{-2}) is generally found in the trade-wind zones of both hemispheres, where strong surface winds of ~8–10 m s^{-1} are associated with large Q_S–Q_{10m} of ~6–7 g kg^{-1}. The larger surface wind speed, Q_S–Q_{10m}, and LHF in the trade-wind belt during the winter than during the summer are due to the stronger wintertime Hadley circulation (Figs. 5–8). In addition, the maximum LHF of ~210–270 W m^{-2} is found in the Kuroshio and Gulf Stream areas (Fig. 8a). Strong surface winds of ~10–12 m s^{-1} coupling with large Q_S–Q_{10m} of ~5–7 g kg^{-1} prevail in these regions during the winters (Figs. 5a, and 7a). This results from the cold, dry continental air with strong offshore winds flowing over the warm oceans in the regions (e.g., Chou and Ferguson 1991; Chou 1993). The LHF and Q_S–Q_{10m} decrease poleward with decreasing SST, with the minima located in high latitudes of the summer hemisphere. In the equatorial eastern Pacific and Atlantic for all seasons, the LHF and Q_S–Q_{10m} are also found to decrease eastward with decreasing SST due to upwelling induced cold SST. The large-scale patterns and seasonal variations of the LHF are similar to those of GSSTF1, HOAPS, and J–OFURO (Chou et al. 1997; Schulz et al. 1997; Kubota et al. 2002a, 2002b).

5. Comparison of LHF with other datasets

The surface turbulent fluxes are derived using various bulk flux algorithms from surface winds, surface air humidity and temperature, and SST, all of which may have a large uncertainty in the reanalyses (based on fixed versions of atmospheric GCMs and data assimilation systems), satellite retrievals, and COADS. Smith et al. (2001) quantified the uncertainties in the NCEP/NCAR reanalysis (referred to as NCEP) by comparing the 1990–95 turbulent fluxes and input variables of NCEP with those collocated (space and time) measurements by research ships during the World Ocean Circulation Experiment (WOCE). Wang and McPhaden (2001) compared six state-of-the-art surface heat flux products (including three reanalysis fields) in the equatorial Pacific with heat fluxes computed from Tropical Atmosphere-Ocean (TAO) buoy data.

There is no "ground truth" for the global flux fields; thus the intercomparison studies are required to assess the sources of errors for various global flux products. The studies can identify the strengths and weaknesses of various flux products, and provide important information for improving atmospheric GCMs and satellite retrievals. As NCEP and da Silva et al. (1994, referred to as da Silva) have been widely used for various studies, it is important to include them for the comparison. Kubota et al. (2002b) compared the 1992–94 LHF derived from GSSTF1, HOAPS, J-OFURO, NCEP, and ECMWF (the European Centre for Medium–Range Weather Forecasts) analysis, as well as the 1992–93 LHF of da Silva, over the global oceans. They found that the large-scale patterns of the LHF are generally similar but with quantitative differences among various products. In this study we compare 1992–93 monthly LHF and input parameters among GSSTF1, GSSTF2, HOAPS, NCEP, and da Silva. To evaluate the differences among various flux products, only the space and time matched monthly mean valid data for the common period of 1992–93 are used for the comparison. Thus this study is different from Kubota et al (2002b).

Figure 9 shows zonal averages of the LHF, 10-m wind speed, and sea-air humidity difference (Q_s–Q_a) over global oceans during 1992–93 for GSSTF2, HOAPS, NCEP, and da Silva, respectively. Figure 10 shows zonal averages of the differences of HOAPS, NCEP, and da Silva from GSSTF2 for these parameters during the same period. To properly compare the wind speed at the 10-m height, the 20-m wind speed of da Silva is multiplied by 0.94 to reduce to that at the 10-m height. However, the surface air specific humidity (Q_a) is not adjusted. The reference heights of

Q_a are 10 m for GSSTF2 and HOAPS, 2 m for NCEP, and 20 m for da Silva. The saturation specific humidity at the sea surface (Q_s) includes a 2% reduction due to the salinity effect for GSSTF2, HOAPS, and da Silva, but not for NCEP. It is noted that the 2-m Q_a is generally larger than that at the 10-m height by ~0.6 g kg^{-1} for the Q_s–Q_a of 5 g kg^{-1} and by ~0.1 g kg^{-1} for the Q_s–Q_a of 1 g kg^{-1}. The humidity difference at the 10-m and 20-m heights is generally negligible. Thus the differences in the surface air humidity shown in Fig. 10c are mainly due to the Q_a differences rather than the differences in the reference heights. Note that the results for GSSTF1 are not shown in Figs. 9 and 10. This is because the differences between GSSTF1 and GSSTF2 are generally negligibly small, except for the LHF. The LHF averaged over the oceans within 60°S–60°N (referred to as the global average) is 12.7 W m^{-2} larger for GSSTF1, as compared to GSSTF2. This difference (~12% of the global average LHF for GSSTF2) is mainly due to the difference in the von Karman constant of humidity between GSSTF1 (0.45) and GSSTF2 (0.40) as discussed in the appendix.

Figure 9a shows that the LHF, for the four flux products, has the maximum in the trade-wind regions of both hemispheres and decreases equatorward and poleward, with the minimum near the equator and high latitudes. However, there are significant differences among them (Figs. 9a and 10a). The NCEP LHF appears to agree with that of GSSTF2 within ~10 W m^{-2}, except a negative bias of –20 W m^{-2} in the 40–60°S band. The LHF of da Silva is smaller than that of GSSTF2 but with the difference of <10 W m^{-2}, except for the equatorial region (larger with the difference up to ~20 W m^{-2}) and the Southern Oceans (smaller by 20–40 W m^{-2}). The HOAPS has the lowest LHF in the tropics among the four flux products. Compared to GSSTF2, the HOAPS LHF is smaller by 20–50 W m^{-2} in the tropics. The discrepancy in the LHF among GSSTF2, HOAPS, and da Silva is primarily caused by the differences in the input variables, as the moisture transfer coefficients used are very close. However, the situation is not true for NCEP. The moisture transfer coefficient of NCEP is significantly larger than that of GSSTF2 (or the other two flux datasets; Zeng et al. 1998), which effect appears to offset the effects of weaker winds and smaller sea-air humidity difference on the LHF (Figs. 9 and 10). Thus, the latent heat fluxes of NCEP and GSSTF2 appear to be generally in good agreement.

Figure 9b shows that the surface (10 m) wind speed, for the four datasets, has the minimum at the equator and increases poleward, with the primary (secondary) maximum near 50° (in the trade-wind belts) of both hemispheres. However, the NCEP 10-m wind speed is weaker with the difference reaching 1.2 m s^{-1} in the 40°S–40°N region but is stronger with the difference up to 0.5 m s^{-1} poleward of 40°, when compared with GSSTF2 (Fig. 10b). The negative bias of NCEP wind speed in the tropics is consistent with the findings of Meissner et al. (2001) and Wang and McPhaden (2001), who compared the NCEP winds with TAO data. The HOAPS also has weaker winds in the tropics of 30°S–30°N (the difference up to 1.5 m s^{-1}) but has stronger winds in the extratropics (the difference up to 1.5 m s^{-1}), as compared to GSSTF2. The da Silva 10-m wind speed is generally within 0.5 m s^{-1} of GSSTF2, except is higher by ~1 m s^{-1} near 20°N and is stronger by 1–2.5 m s^{-1} in the 40–60°N band. Meissner et al. (2001) found that the SSM/I surface winds are higher than those of buoy measurements by 0.15 m s^{-1}, with a SD error of 1.29 m s^{-1}. Their results are consistent with Fig. 2a, which shows that the GSSTF2 surface wind speed has a positive bias of 0.36 m s^{-1} and a SD error of 1.38 m s^{-1}, with a slightly higher bias for the high-wind cases when compared with the ship measurements. Thus, it is very likely that the GSSTF2 wind speed is more accurate and the differences in the wind speed shown in Figs. 9b and 10b are primarily caused by the errors in HOAPS, NCEP, and da Silva.

Da Silva et al. (1994) assumed an anemometer height of 20 m to the entire wind dataset measured by ship anemometers of COADS to derive a Beaufort equivalent scale for determining visual wind speeds, which depend on sea states. However, Kent and Taylor (1997) found that the true anemometer heights had large standard deviations with the means generally much higher than 20 m and increasing with time. For example, they found that the mean anemometer height was 35.2 m (24.2 m) with a standard deviation of 8.4 m (10.9 m) in middle latitudes of the North Pacific (North Atlantic) during 1990. An underestimation of anemometer height can cause unrealistic higher ship anemometer-measured (and visual) wind speeds, because the higher wind speeds measured at the higher anemometer heights are assigned to the assumed lower levels. For the same error of anemometer height, the stronger the wind is, the larger the wind speed error is. This can cause a larger discrepancy of wind speeds in the high-wind regions. This is likely to be the major

reason that a large discrepancy of wind speeds in the high-wind region of the northern high latitudes is found between da Silva and GSSTF2.

Figure 9c shows that the sea-air humidity difference (Q_s–Q_a) is higher in the tropics and decreases poleward. However, the meridional profiles of Q_s–Q_a are quite different in the tropics among the four products. The Q_s–Q_a of GSSTF2 and HOAPS has the maximum in the trade-wind regions and decreases equatorward and poleward, while that of NCEP and da Silva generally has the maximum near the equator and decrease poleward. The discrepancy in Q_s–Q_a is mainly due to the difference in Q_a. This can be clearly seen from Fig. 10c and 10d, which show the differences in Q_a and Q_s for the four datasets, respectively. The GSSTF2 has the smallest Q_s. However, the differences in Q_s among the four datasets are generally very small (<0.5 g kg^{-1}), which arise from the differences in the SST, sea-level pressure, and formula for computing Q_s. Figure 10c shows that the NCEP 2-m Q_a is wetter than the GSSTF2 10-m Q_a by ~1–1.7 g kg^{-1} in the regions poleward of ~10°, with decreased differences near the equator. The 20-m Q_a of da Silva is wetter than the GSSTF2 10-m Q_a by ~0.5–1.7 g kg^{-1} in the regions poleward of ~10°, with small differences (<0.5 g kg^{-1}) near the equator. The HOAPS 10-m Q_a is wetter than the GSSTF2 10-m Q_a by ~0.4–1.3 g kg^{-1}, with significant differences of 1–1.3 g kg^{-1} within ~15° of the equator.

Since there is no ground truth for the global surface air humidity, we analyze the humidity discrepancies based on Table2, Fig. 2b, and previous studies. Table 2 shows that the GSSTF2 Q_a has a positive bias of ~1 (~0.7) g kg^{-1} in the tropical oceans (for the nine experiments over the tropical and midlatitude oceans). Figure 2b shows that the GSSTF2 Q_a has a positive bias for the moist region with the humidity of ~16–20 g kg^{-1} but has a small negative bias for the dry region with the humidity of ~3–6 g kg^{-1}. Smith et al. (2001) and Wang and McPhaden (2001) found that the NCEP surface air humidity had positive biases when compared with those measured by research ships and TAO buoys. Their results and this study imply that the GSSTF2–NCEP humidity difference shown in Fig.10c is mostly due to the moist bias of NCEP. Previous studies (e.g., da Silva et al. 1994; Chou et al. 1997; Josey et al. 1999) found that ship observations overestimated dew point temperatures (by ~0.5°C), which resulted in moist bias of the surface air

humidity for COADS, and thus for da Silva. Their results and this study suggest that the GSSTF2–da Silva humidity difference shown in Fig. 10c is mostly due to the moist bias of da Silva. The results also suggest that the surface air humidity of HOAPS is significantly overestimated in the tropical oceans, as it is larger than the moist biased GSSTF2 humidity. These analyses suggest that the GSSTF2 surface air humidity is likely to be closest to the reality among the four datasets analyzed, although it is still subject to regional biases.

Table 3 compares the averages of LHF and input parameters for the global oceans (60°S–60°N), northern extratropical oceans (20°N–60°N), tropical oceans (20°S–20°N), and southern extratropical oceans (20°S–60°S) during 1992–93 among GSSTF2, HOAPS, NCEP, and da Silva. The global-mean LHF are 108.2, 88.5, 104.8, and 99.7 W m^{-2}, respectively, for GSSTF2, HOAPS, NCEP, and da Silva. The global-mean LHF is the largest for GSSTF2 and the smallest for HOAPS, with a difference of 20 W m^{-2}. Over the tropical oceans, the HOAPS LHF has the maximum difference (37 W m^{-2}) from that of GSSTF2, whereas the other two datasets are comparable. This is mainly a result of weaker winds (weaker by ~1 m s^{-1}) coupling with smaller sea-air humidity difference (smaller by ~0.7 g kg^{-1}). The significant overestimation (wetter than GSSTF2 by 1.1 g kg^{-1}) of the surface air humidity in the tropical oceans is primarily the cause for the latter. The global-mean LHF of NCEP is comparable to that of GSSTF2, but the sea-air humidity difference and surface wind are weaker (by 0.8 g kg^{-1} and 0.6 m s^{-1}), which appear to offset the larger moisture transfer coefficient (Zeng et al. 1998). The LHF of da Silva is generally comparable to that of GSSTF2, except for the southern extratropical oceans. Over the southern extratropical oceans, the LHF of da Silva is the smallest among the four datasets, with a negative bias of 22 W m^{-2} as compared to GSSTF2. This discrepancy is most likely due to the errors arising from the interpretation of missing data in the large data-void southern extratropical oceans. In short, our analyses suggest that the GSSTF2 latent heat flux, surface air humidity, and winds are likely to be more realistic than the other four datasets analyzed, although those of GSSTF2 are still subject to regional biases. More high-quality observations over the global oceans are vital to do a more detailed regional validation, to improve satellite retrieval, and to further confirm this conclusion.

6. Concluding remarks

The GSSTF2 is a 13.5-year (July 1987–December 2000) global dataset of daily ocean surface turbulent fluxes of momentum, heat, and moisture, with 1° spatial resolution. Turbulent fluxes are derived from the SSM/I surface winds (Wentz 1997) and surface air humidity (Chou et al. 1995, 1997), as well as the SST and 2-m air temperature of the NCEP/NCAR reanalysis, based on the method of Chou et al. (1997) with two improvements (salinity effect for the Q_s and von Karman constant). The directions of wind stress are taken from those of the surface winds, which are derived from a blend of the SSM/I surface wind speeds (Wentz 1997), surface wind vectors from ships, buoys, and NCEP/NCAR reanalysis following the method of Atlas et al. (1996).

Hourly fluxes computed from the GSSTF2 bulk aerodynamic algorithm using the observed hourly input variables validate well against those of ten field experiments conducted by the NOAA/ETL (Fairall et al. 1996a; 1997) research ships over the tropical and midlatitude oceans during 1991–99. Compared to the ten experiments, the computed hourly wind stress has a negative bias of –0.0005 N m^{-2}, a SD error of 0.0106 N m^{-2}, and a correlation of 0.98. The computed hourly latent heat flux (LHF) has a bias of 4.5 W m^{-2}, a SD error of 19.6 W m^{-2}, and a correlation of 0.91. The computed hourly sensible heat flux (SHF) has a negative bias of –0.2 W m^{-2}, a SD error of 7.3 W m^{-2}, and a correlation of 0.82. The computed sensible heat flux appears to have lower accuracy, compared to the computed wind stress and latent heat flux. This is most likely due to the fact that the small SHF is more sensitive to measurement and parameterization errors. Overall the results suggest that the GSSTF2 bulk scheme is generally accurate for weak and moderate winds, but slightly underestimates the LHF and SHF for strong-wind cases.

The GSSTF2 daily wind stress, latent heat flux, wind speed, surface air humidity and SST compare reasonably well with those collocated with nine field experiments. Compared to the nine field experiments, the GSSTF2 daily wind stress has a positive bias of 0.0129 N m^{-2}, a SD error of 0.0774 N m^{-2}, and a correlation of 0.72. The daily LHF has a bias of 0.8 W m^{-2}, a SD error of 35.8 W m^{-2}, and a correlation of 0.83. The daily SHF has a positive bias of 6.4 W m^{-2}, a SD error of

10.1 W m^{-2}, and a correlation of 0.84. The daily surface wind speed has a bias of 0.36 m s^{-1}, a SD error of 1.38 m s^{-1}, and a correlation of 0.92. The daily surface air specific humidity has a bias of 0.67 g kg^{-1}, a SD error of 1.23 g kg^{-1}, and a correlation of 0.97. The daily surface air temperature has a negative bias of –0.47°C, a SD error of 0.82°C, and a correlation of 0.99. The daily SST has a negligible bias of 0.04°C, a SD error of 0.51°C, and a correlation of 1.0. In addition, the global distributions of 1988–2000 annual- and seasonal-mean turbulent fluxes show reasonable patterns related to the atmospheric general circulation and seasonal variations.

Zonal averages of LHF and input parameters over global oceans during 1992–93 are compared among the GSSTF1, GSSTF2, HOAPS, NCEP/NCAR reanalysis, and da Silva et al. (1994). Our analyses suggest that the GSSTF2 latent heat flux, surface air humidity, and winds are likely to be more realistic than the other four flux products examined, although those of GSSTF2 are still subject to regional biases. More high-quality observations over the global oceans are vital to do a more detailed regional validation, to improve satellite retrieval, and to further confirm our conclusion. The GSSTF2 derived from the SSM/I is useful for climate studies and is available at http://daac.gsfc.nasa.gov/CAMPAIGN_DOCS/hydrology/hd_gsstf2.0.html. We plan to produce a 0.25° dataset of surface turbulent fluxes over the global ocean using the newly improved version-5 SSM/I data of Wentz with a new bulk flux scheme with additional improvement for the high-wind conditions. The dataset will be used for pixel validation of fluxes and input variables.

Acknowledgments This study is supported by the TRMM Program and Physical Oceanography Program, NASA/Office of Earth Science. The first author is especially grateful to R. Kakar, the TRMM Program Manager, and R. Adler, the TRMM Project Scientist, for their continuous support and encouragement. The SSM/I version-4 data of total precipitable water, wind speeds, and antenna temperatures produced by F. Wentz's group are obtained from http://www.ssmi.com. The NCEP/NCAR reanalysis data are obtained from the NOAA/CIRES Climate Diagnostics Center at http://www.cdc.noaa.gov/. The flux data of the NOAA/ETL research ships processed by C.

Fairall's group are obtained from the SEAFLUX web site at http://paos.colorado.edu/~curryja/ocean/. The HOAPS data are obtained from http://www.mpimet.mpg.de/Depts/Physik/HOAPS/. The COADS turbulent fluxes are provided by A. da Silva. Consultation related to the computer codes of the Wentz SSM/I antenna temperatures has been provided by G. J. Huffman. The GSSTF1 and GSSTF2 are archived at the NASA/GSFC DAAC through the help of L. Chiu and W. L. Teng.

APPENDIX

The GSSTF2 Bulk Aerodynamic Algorithm and Validation

a. Algorithm

The GSSTF2 bulk aerodynamic algorithm is based on that of GSSTF1 (Chou et al. 1997; Chou 1993) with two modifications. Chou (1993) discussed that bulk scheme in detail; thus we first briefly describe the algorithm and then discuss the modifications. The roughness lengths for momentum (z_o), heat (z_{ot}), and moisture (z_{oq}) are parameterized as:

$$z_o = 0.0144 \frac{u_*^2}{g} + 0.11 \frac{\nu}{u_*} \tag{A1}$$

$$z_{ot} \frac{u_*}{\nu} = a_1 \mathrm{Re}_*^{b_1} \tag{A2}$$

$$z_{oq} \frac{u_*}{\nu} = a_2 \mathrm{Re}_*^{b_2} , \tag{A3}$$

where u_* is the friction velocity, g the gravitational acceleration, ν the kinematic viscosity of air, Re_*(= $z_o u_* / \nu$) the roughness Reynolds number, and a_1, a_2, b_1, and b_2 the coefficients that depend on Re_* and are given in Table 1 of Liu *et al.* (1979). Note that the roughness lengths z_{ot} and z_{oq} are essentially the same as those of the COARE algorithm (version 2.5; Fairall et al. 1996a), but the first term of z_o (A1) is slightly larger than that of the COARE algorithm (0.0144 verses 0.011). The dimensionless gradients of wind (ϕ_u), potential temperature (ϕ_t), and humidity (ϕ_q) are functions of the stability parameter z/L, where z is the measurement height, and L the Monin–Obukhov length. For the stable situation they are given as:

$$\phi_u = \phi_t = \phi_q = 1 + 7\ z/\mathrm{L}. \tag{A4}$$

For the unstable situation, they are given as:

$$\phi_u = (1 - 16\ z/\mathrm{L})^{-1/4}, \tag{A5}$$

$$\phi_t = \phi_q = (1-16\ z/L)^{-1/2}. \qquad \text{(A6)}$$

Using the Monin-Obukhov similarity theory and above dimensionless gradients, both schemes derive the turbulent fluxes from the surface-layer scaling parameters by iteratively solving the diabatic profiles of wind, temperature, and humidity. The bulk transfer coefficients are stability dependent and are functions of wind speed, and sea-air temperature and humidity differences.

There are two differences between these two schemes. The saturation specific humidity at the sea surface, Q_S, for the GSSTF2 is computed as $Q_S = 0.98\ (0.622\ e/P)$, where e is the saturation vapor pressure for pure water at the bulk SST, and P is the sea level pressure. This includes the 2% reduction in the saturation vapor pressure for saline water as compared to pure water (Fairall et al. 1996a; Zeng et al. 1998), while the approximated formulation of the specific humidity is intended to partially compensate the cool skin effect. On the other hand, the GSSTF1 bulk scheme does not include the salinity effect and sets $Q_S = (0.622\ e/P)$ to partially compensate the cool skin effect. In addition, the GSSTF2 bulk flux scheme assumes the same von Karman constants of 0.4 for velocity, temperature, and humidity following Fairall et al. (1996a, 1997), while the GSSTF1 scheme adopts different von Karman constants of 0.4, 0.36, and 0.45, respectively (Chou 1993). The neutral transfer coefficients (at the10-m height) of momentum, heat, and moisture for the GSSTF2 are 1.02–1.81 $x10^{-3}$, 1.01–1.18 x 10^{-3}, and 1.05–1.22 x 10^{-3}, respectively, for the 10-m wind speed of 3–18 m s^{-1}, and increase with decreasing wind speed when wind speeds are less than 3 m s^{-1} (see Chou 1993). The transfer coefficients (for the surface wind up to ~18 m s^{-1}) are in close agreement with those of Zeng et al. (1998), Fairall et al. (1996a), and Renfrew et al. (2002). The change in the von Karman constants causes the GSSTF2 transfer coefficients to decrease 11% for the latent heat flux but to increase 11% for the sensible heat flux, as compared to those of GSSTF1. These two changes in the bulk scheme thus cause the latent heat flux (LHF) to be smaller for GSSTF2 than for GSSTF1, if the input variables remain the same.

b. Validation

Hourly turbulent fluxes are computed from the GSSTF2 bulk aerodynamic algorithm, using hourly wind speed, specific humidity, and temperature of the surface air, and SST (at the 5-cm

depth) measured from the ten field experiments conducted by the NOAA/ETL research ships (Table A1). Table A2 compares hourly ID wind stresses, covariance LHF, and covariance SHF for each of the ten experiments with those computed using the GSSTF2 bulk flux scheme. To see the overall comparison, the scatterplots of the computed versus the observed fluxes for all ten experiments are shown in Fig. A1. Table A2 shows that the turbulent fluxes measured during FASTEX are significantly larger than those of other experiments due to higher winds (reaching ~20 m s^{-1}). On the other hand, the surface turbulent fluxes measured during COARE have been intensively analyzed, and compared by numerous scientists (e.g., Fairall et al. 1996a; Weller and Anderson 1996; Chou et al. 1997, 2000; Schulz et al. 1997; Curry et al. 1999). It is also interesting to know the comparison for these two experiments. Thus, we use different symbols for the comparison in Fig. A1 (F for FASTEX, C for COARE, and X for the rest of the experiments used for the comparison).

It can be seen from Fig. A1 and Table A2 that the hourly wind stress and latent heat flux computed from the GSSTF2 bulk scheme agree very well with those of the observed. Compared to 1913 samples of hourly turbulent fluxes of the ten experiments, the computed hourly wind stress has a negative bias of –0.0005 N m^{-2}, a standard deviation (SD) error of 0.0106 N m^{-2}, and a correlation of 0.98, with a correlation range of 0.91–0.99. The SD error is the standard deviation of the differences between the computed and observed. The computed hourly LHF has a bias of 4.5 W m^{-2}, a SD error of 19.6 W m^{-2}, and a correlation of 0.91, with a correlation range of 0.77–0.95. The computed hourly SHF has a negative bias of –0.2 W m^{-2}, a SD error of 7.3 W m^{-2}, and a correlation of 0.82, with a correlation range of 0.44–0.91. Note that the model-ship differences in hourly turbulent fluxes include errors in the parameterization of the GSSTF2 bulk aerodynamic algorithm, as well as the uncertainty in the input variables and fluxes measured by the ships (e.g., Fairall et al. 1996a). The computed sensible heat flux appears to have lower accuracy, compared to the computed wind stress and latent heat flux. This is most likely due to the fact that the small sensible heat flux is more sensitive to measurement and parameterization errors. Overall the results suggest that the GSSTF2 bulk scheme is generally accurate for weak and moderate winds, but slightly underestimates latent and sensible heat fluxes for strong winds.

REFERENCES

Atlas, R., R. N. Hoffman, S. C. Bloom, J. C. Jusem, and J. Ardizzone, 1996: A multiyear global surface wind velocity dataset using SSM/I wind observations. *Bull. Amer. Meteor. Soc.*, **77**, 869-882.

Chou, S.-H., 1993: A comparison of airborne eddy correlation and bulk aerodynamic methods for ocean-air turbulent fluxes during cold-air outbreaks. *Bound.-Layer Meteor.*, **64**, 75-100.

Chou, S.-H. and M. P. Ferguson, 1991: Heat fluxes and roll circulations over the western Gulf Stream during an intense cold-air outbreak. *Bound.-Layer Meteor.*, **55**, 255-281.

Chou, S.-H., R. M. Atlas, C.-L. Shie and J. Ardizzone, 1995: Estimates of surface humidity and latent heat fluxes over oceans from SSM/I data. *Mon. Wea. Rev.*, **123**, 2405-2425.

Chou, S.-H., C.-L. Shie, R. M. Atlas and J. Ardizzone, 1997: Air-sea fluxes retrieved from Special Sensor Microwave Imager data. *J. Geophys. Res.*, **102**, 12705-12726.

Chou, S.-H., W. Zhao, and M.-D. Chou, 2000: Surface heat budgets and sea surface temperature in the Pacific warm pool during TOGA COARE. *J. Climate,* **13**, 634-649.

Curry, J. A., and co-authors, 1999: High-resolution satellite-derived dataset of the surface fluxes of heat, freshwater, and momentum for the TOGA COARE IOP. *Bull. Amer. Meteor. Soc.*, **80**, 2059-2080.

Curry, J. A., and co-authors, 2002: SEAFLUX. *Bull. Amer. Meteor. Soc.*, (submitted).

da Silva, A, C. C. Young and S. Levitus, 1994: Atlas of Surface Marine Data 1994 Vol. 1: Algorithms and Procedures. NOAA Atlas NESDIS 6, US Dept. of Commerce, NOAA, NESDIS, Washington, DC, 83 pp.

Esbensen, S. K., D. B. Chelton, D. Vickers and J. Sun, 1993: An analysis of errors in Special Sensor Microwave Imager evaporation estimates over the global oceans. *J. Geophys. Res., 98 (C4),* 7081-7101.

Fairall, C., E. F. Bradley, D. P. Rogers, J. B. Edson, and G. S. Young, 1996a: Bulk parameterization of air-sea fluxes for Tropical Ocean Global Atmosphere Coupled Ocean-Atmosphere Response Experiment. *J. Geophys. Res.*, **101** (C2), 3747-3764.

Fairall, C. W., E. F. Bradley, J. S. Godfrey, J. B. Edson, and G. S. Young, and G. A. Wick, 1996b: Cool-skin and warm-layer effects on sea surface temperature, *J. Geophys. Res.*, **101**, 1295-1308.

Fairall, C. W., A. B. White, J. B. Edson, and J. E. Hare, 1997: Integrated shipboard measurements of the marine boundary layer. *J. Atmos. Oceanic Technol.*, **14**, 338-359.

Hellerman , S. and M. Rosenstein, 1983: Normal monthly wind stress over the world ocean with error estimates. *J. Phys. Oceanogr.*, **13**, 1093-1104.

Josey, S. A., E. C. Kent and P. K. Taylor 1999: New insights into the ocean heat budget closure problem from analysis of the SOC air-sea flux climatology. *J. Climate*, **12**, 2856 - 2880.

Kalnay, E., and co-authors, 1996: The NCEP/NCAR 40-year reanalysis project. *Bull. Amer. Meteor. Soc.*, **77**, 437-471.

Kent, E. C., and P. K. Taylor, 1997: Choice of a Beaufort equivalent scale. *J. Atmos. Oceanic Technol.*, **14**, 228-242.

Kubota, M., K. Ichikawa, N. Iwasaka, S. Kizu, M. Konda, and K. Kutsuwada, 2002a: Japanese Ocean Flux Data Sets with Use of Remote Sensing Observations (J-OFURO) introducing J-OFURO. *J. Oceanogr.*, **58**, 213-215.

Kubota, M., A. Kano, H. Muramatsu and H. Tomita, 2002b: Intercomparison of various surface latent heat flux fields. J. Climate (submitted).

Liu, W. T., K. B. Katsaros, and J. A. Businger, 1979: Bulk parameterization of air-sea exchanges of heat and water vapor including the molecular constraints at the interface. *J. Atmos. Sci.*, **36**, 1722-1735.

Meissner,T., D.Smith, and F.J.Wentz, 2001: A 10-year intercomparison between collocated SSM/I oceanic surface wind speed retrievals and global analyses. *J. Geophys. Res.*, **106**, 11731-11742,

Renfrew, I.A., G.W.K. Moore, P.S. Guest, and K. Bumke, 2002: A comparison of surface layer and surface turbulent flux observations over the Labrador Sea with ECMWF analyses and NCEP reanalyses. *J. Phys. Oceanogr.*, **32**, 383-400.

Reynolds, R. W. and T. S. Smith, 1994: Improved global sea surface temperature analyses. *J. Climate.*, **7**, 929-948.

Schulz, J., P. Schluessel and H. Grassl, 1993: Water vapor in the atmospheric boundary layer over oceans from SSM/I measurements. *Int. J. Rem. Sens.*, **14**, 2773-2789.

Schulz, J., J. Meywerk, S. Ewald, and P. Schluessel, 1997: Evaluation of satellite-derived latent heat fluxes. *J. Climate*, **10**, 2782-2795.

Smith, S. R., D. M. Legler, and K. V. Verzone, 2001: Quantifying uncertainties in NCEP reanalyses using high-quality research vessel observations. *J. Climate.* **14**, 4062-4072.

Wang, W., and M. J. McPhaden, 2001: What is the mean seasonal cycle of surface heat flux in the equatorial Pacific? *J. Geophys. Res.*, **106**, 837-857.

Webster, P., C. A. Clayson, and J. A. Curry, 1996: Clouds, radiation, and the diurnal cycle of sea surface temperature in the tropical western Pacific. *J. Climate*, **9**, 1712-1730.

Weller R. A. and S. P. Anderson, 1996: Surface meteorology and air-sea fluxes in the western equatorial Pacific warm pool during the TOGA Coupled Ocean-Atmosphere Response Experiment. *J. Climate,* **9**, 1959-1990.

Wentz, F. J., 1997: A well calibrated ocean algorithm for SSM/I. *J. Geophys. Res.*, **102**, 8703-8718.

Wick, G. A., W. J. Emery and L. H. Kantha, 1996: The behavior of the bulk-skin sea surface temperature difference under varying wind speed and heat flux. *J. Phys. Oceanogr.* **26**, 1969-1988.

Woodruff, S. D., S. J. Lubker, K. Wolter, S. J. Worley, and J. D. Elm, 1993: Comprehensive Ocean-Atmosphere Data Set (COADS) release 1a: 1980-92. *Earth Syst. Monit.*, **4**, 4-8.

Yelland, M., B. I. Moat, P. K. Taylor, R. W. Pascal, J. Hutching, and V. C. Cornell, 1998: Wind stress measurements from the open ocean corrected for airflow distortion by the ship. *J. Phys. Oceanogr.*, **28**, 1511-1526.

Zeng, X., M. Zhao, and R. E. Dickinson, 1998: Intercomparison of bulk aerodynamic algorithms for the computation of sea surface fluxes using TOGA COARE and TAO data. *J Climate*, **11**, 2628-2644.

Table 1. Approximate local times (LT) of equatorial crossing and data records for each SSM/I of the DMSP satellites used in the derivation of GSSTF2.

Satellites	Equatorial crossing (LT)	Data records
DMSP F08	0615/1815	1987/7/9– 1991/12/31
DMSP F10	0945/2145	1991/1/1– 1997/11/14
DMSP F11	0600/1800	1992/1/1– 1996/12/31
DMSP F13	0600/1800	1995/5/3– 2000/12/31
DMSP F14	0845/2045	1997/5/8– 2000/12/31

Table 2. Comparison of daily wind stress, latent heat fluxes (LHF), sensible heat fluxes (SHF), surface wind speed (wspd), surface air humidity (Q_a), surface air temperature (T_a), and SST of GSSTF2 with those of all nine experiments and five tropical experiments with large samples observed by the NOAA/ETL research ships. The mean is ship-observed values averaged over collocated days, positive bias indicates larger GSSTF2, SD error is standard deviation of differences, and r is correlation coefficient. Units are 10^{-3} N m^{-2} for wind stress, W m^{-2} for heat fluxes, m s^{-1} for wspd, g kg^{-1} for Q_a and °C for T_a and SST.

Source	Days	Variable	Mean	Bias	SD error		r
					Daily	Monthly	
all	167	stress	54.1	12.9	74.4	13.6	0.72
Tropics	134	stress	32.7	5.3	19.3	3.5	0.81
all	167	LHF	99.8	0.8	35.8	6.5	0.83
Tropics	134	LHF	93.0	–2.6	29.7	5.4	0.80
all	167	SHF	8.9	6.4	10.1	1.8	0.84
Tropics	134	SHF	5.5	7.0	6.2	1.1	0.45
all	240	wspd	5.9	0.36	1.38	0.25	0.92
Tropics	139	wspd	4.6	0.31	1.07	0.20	0.87
all	240	Q_a	15.7	0.67	1.23	0.22	0.97
Tropics	139	Q_a	17.7	1.01	1.11	0.20	0.85
all	240	T_a	24.6	–0.47	0.82	0.15	0.99
Tropics	139	T_a	27.2	–0.70	0.76	0.14	0.94
all	279	SST	25.7	0.04	0.51	0.09	1.00
Tropics	157	SST	28.4	0.02	0.30	0.05	0.99

Table 3. Regional-mean latent heat fluxes (LHF), 10-m wind speeds (U_{10m}), surface air specific humidity (Q_a), surface saturation specific humidity (Q_s), and sea-air humidity differences (Q_s–Q_a) over global oceans during 1992-93 for GSSTF2, HOAPS, NCEP, and da Silva.

Variable	Source	60°S–60°N	20°N–60°N	20°S–20°N	20°S–60°S
LHF	GSSTF2	108.2	104.1	122.1	94.3
(W m^{-2})	HOAPS	88.5	89.8	84.7	92.3
	NCEP	104.8	104.6	125,1	81.1
	Da Silva	99.7	98.8	123.4	72.5
U_{10m}	GSSTF2	7.4	7.3	6.6	8.3
(m s^{-1})	HOAPS	7.1	7.6	5.5	8.7
	NCEP	6.8	7.1	5.6	8.0
	Da Silva	7.6	8.1	6.8	8.3
Q_a	GSSTF2	12.1	10.2	16.6	7.8
(g kg^{-1})	HOAPS	12.9	10.9	17.7	8.4
	NCEP	13.2	11.4	17.5	9.2
	Da Silva	12.9	11.2	17.1	8.9
Q_s	GSSTF2	16.2	14.0	21.7	11.0
(g kg^{-1})	HOAPS	16.6	14.3	22.1	11.4
	NCEP	16.6	14.3	22.2	11.2
	Da Silva	16.6	14.5	22.1	11.4
Q_s–Q_a	GSSTF2	4.1	3.8	5.1	3.2
(g kg^{-1})	HOAPS	3.7	3.4	4.4	3.0
	NCEP	3.3	2.9	4.6	2.1
	Da Silva	3.7	3.2	5.0	2.6

Table A1. Times and locations of ten field experiments conducted by the NOAA/ETL research ships.

Experiments	Times	Locations
ASTEX	92/6/6–92/6/28	30°N, 36°W
COARE	92/11/11–93/2/16	1.7°S, 156°E
FASTEX	96/12/22–97/1/26	42–52°N, 5–60°W
JASMINE	99/5/4–99/5/31	5°S–13°N, 88–98°E
KWAJEX	99/7/28–99/9/10	9°N, 167°E
MOORINGS	99/9/14–99/10/21	8°N, 167°E–49°N, 130°W
NAURU99	99/6/15–99/7/18	12°S, 130°E–8°N, 167°E
PACSF 99	99/11/2–99/12/1	8°S–12°N, 95–121°W
SCOPE	93/9/17–93/9/28	33°N, 118°W
TIWE	91/11/21–91/12/13	0°N, 140°W

Table A2. Comparison of hourly (50-min) ID wind stresses, covariance latent heat fluxes (LHF), and covariance sensible heat fluxes (SHF) for each of ten experiments observed by the NOAA/ETL research ships with those computed using GSSTF2 bulk flux algorithm. The mean is the average observed fluxes for N samples of the experiment, positive bias indicates larger computed fluxes, SDE is standard deviation error, and r is correlation coefficient. Units are 10^{-3} N m^{-2} for wind stress, and W m^{-2} for heat fluxes.

Experiment	N	Stress				LHF				SHF			
		mean	bias	SDE	r	mean	bias	SDE	r	Mean	bias	SDE	r
ASTEX	109	47.8	–3.6	7.8	0.97	64.7	15.1	13.1	0.87	4.8	1.6	2.5	0.84
COARE	565	36.5	–1.0	6.1	0.99	103.3	2.6	21.3	0.89	7.5	–0.8	3.9	0.79
FASTEX	92	215	–4.7	33.9	0.98	150.9	–10.1	32.7	0.93	41.7	–13.6	25.2	0.77
JASMINE	121	36.4	–3.0	13.1	0.95	92.9	15.3	24.0	0.77	4.9	0.2	3.8	0.62
KWAJEX	451	32.6	2.5	5.8	0.97	92.9	3.0	14.9	0.84	5.4	1.1	3.3	0.57
MOORINGS	89	38.2	0.5	9.6	0.93	91.7	8.7	16.6	0.90	4.0	2.7	3.3	0.60
NAURU99	232	30.8	2.0	7.3	0.96	104.7	5.2	19.0	0.89	4.7	0.8	3.8	0.44
PACSF99	10	66.2	–6.1	10.0	0.96	115.1	–4.6	24.5	0.90	8.2	4.3	3.3	0.91
SCOPE	232	31.1	–2.9	7.1	0.98	48.1	5.2	10.7	0.95	13.7	0.8	4.7	0.85
TIWE	12	70.8	–9.5	9.9	0.91	117.5	1.7	16.8	0.85	0.8	2.7	2.7	0.56
All	1913	43.9	–0.5	10.6	0.98	93.4	4.5	19.6	0.91	8.5	–0.2	7.3	0.82

FIGURE CAPTIONS

Fig. 1. Comparison of GSSTF2 daily fluxes with (a) ID wind stresses, (b) covariance latent heat fluxes, and (c) covariance sensible heat fluxes of nine experiments. The symbol C is for COARE, F for FASTEX, and X for the other seven experiments.

Fig. 2. Comparison of GSSTF2 daily (a) winds, (b) specific humidity, and (c) temperatures of surface air with those of nine experiments. The symbols are the same as Fig. 1.

Fig. 3. Annual mean (a) 10-m wind speed, (b) sea–10m humidity difference, and (c) SST–2m temperature difference, averaged over 1988–2000 for GSSTF2.

Fig. 4. Annual mean (a) wind stress, (b) latent heat flux, and (c) sensible heat flux, averaged over 1988–2000 for GSSTF2. Arrows indicate wind stress directions.

Fig. 5. Seasonal mean 10-m wind speeds for (a) DJF, (b) MAM, (c) JJA, and (d) SON, averaged over 1988–2000 for GSSTF2.

Fig. 6. Same as Fig. 5, except for wind stresses. Arrows indicate wind stress directions.

Fig. 7. Same as Fig.5, except for sea–10m humidity differences.

Fig. 8. Same as Fig.5, except for latent heat fluxes.

Fig. 9. Zonal averages of (a) latent heat fluxes, (b) 10-m wind speeds, and (c) sea-air humidity differences over global oceans during 1992–93 for GSSTF2, HOAPS, NCEP, and da Silva. Only the collocated monthly valid data from all four datasets are used.

Fig. 10. Zonal averages of differences of HOAPS, NCEP, and da Silva from GSSTF2 for (a) latent heat fluxes, (b) 10-m wind speeds, (c) surface air specific humidity, and (d) surface saturation specific humidity over global oceans during 1992–93. Only the collocated monthly valid data from all four datasets are used.

Fig. A1. Comparison of hourly fluxes computed using GSSTF2 bulk aerodynamic algorithm with (a) ID wind stresses, (b) covariance latent heat fluxes, and (c) covariance sensible heat fluxes of ten experiments. The symbol C is for COARE, F for FASTEX, and X for other eight experiments.

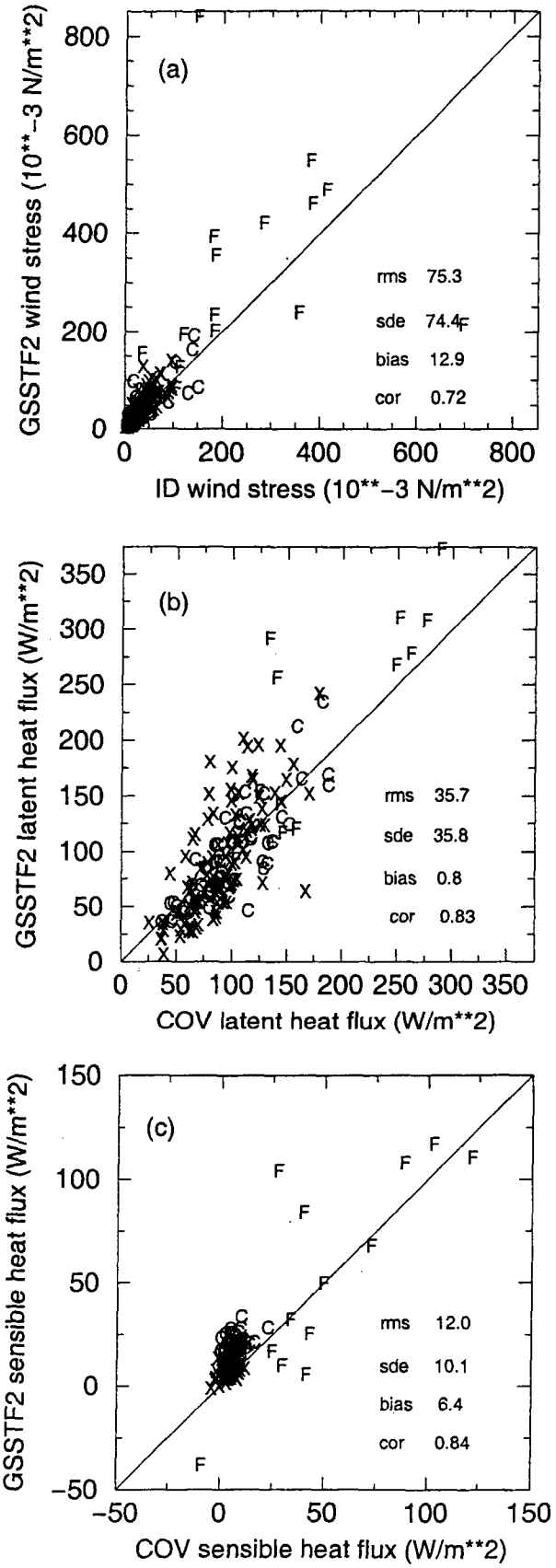
(a)
GSSTF2 wind stress (10**-3 N/m**2)
ID wind stress (10**-3 N/m**2)
rms 75.3
sde 74.4
bias 12.9
cor 0.72
(b)
GSSTF2 latent heat flux (W/m**2)
COV latent heat flux (W/m**2)
rms 35.7
sde 35.8
bias 0.8
cor 0.83
(c)
GSSTF2 sensible heat flux (W/m**2)
COV sensible heat flux (W/m**2)
rms 12.0
sde 10.1
bias 6.4
cor 0.84

Fig. 1

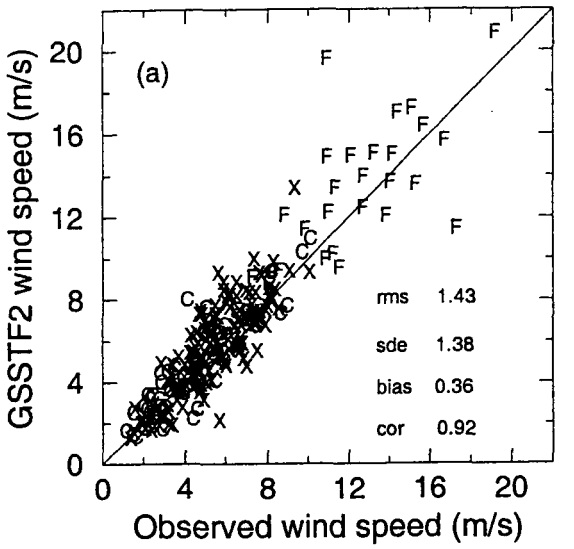
(a)
GSSTF2 wind speed (m/s)
Observed wind speed (m/s)
rms 1.43
sde 1.38
bias 0.36
cor 0.92
0
4
8
12
16
20

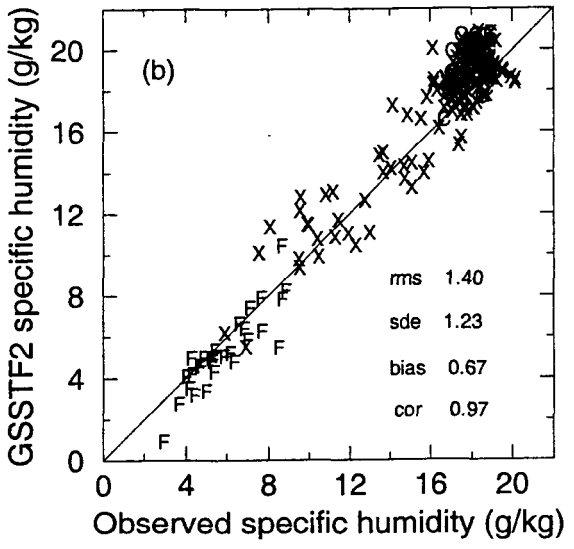
(b)
GSSTF2 specific humidity (g/kg)
Observed specific humidity (g/kg)
rms 1.40
sde 1.23
bias 0.67
cor 0.97
0
4
8
12
16
20

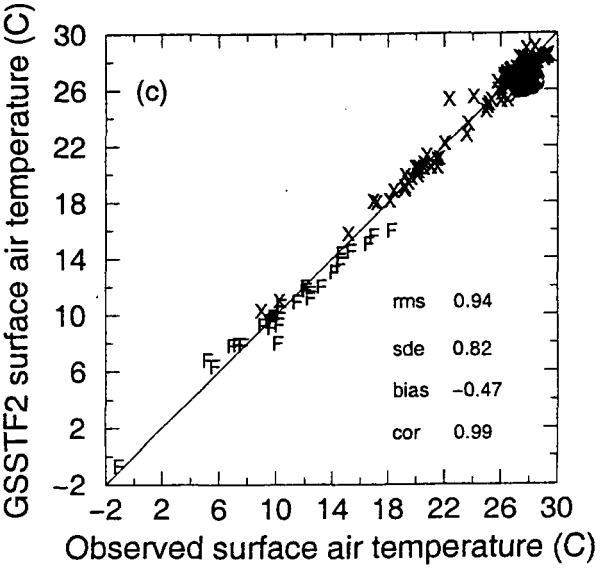
(c)
GSSTF2 surface air temperature (C)
Observed surface air temperature (C)
rms 0.94
sde 0.82
bias -0.47
cor 0.99
-2
2
6
10
14
18
22
26
30

Fig 2

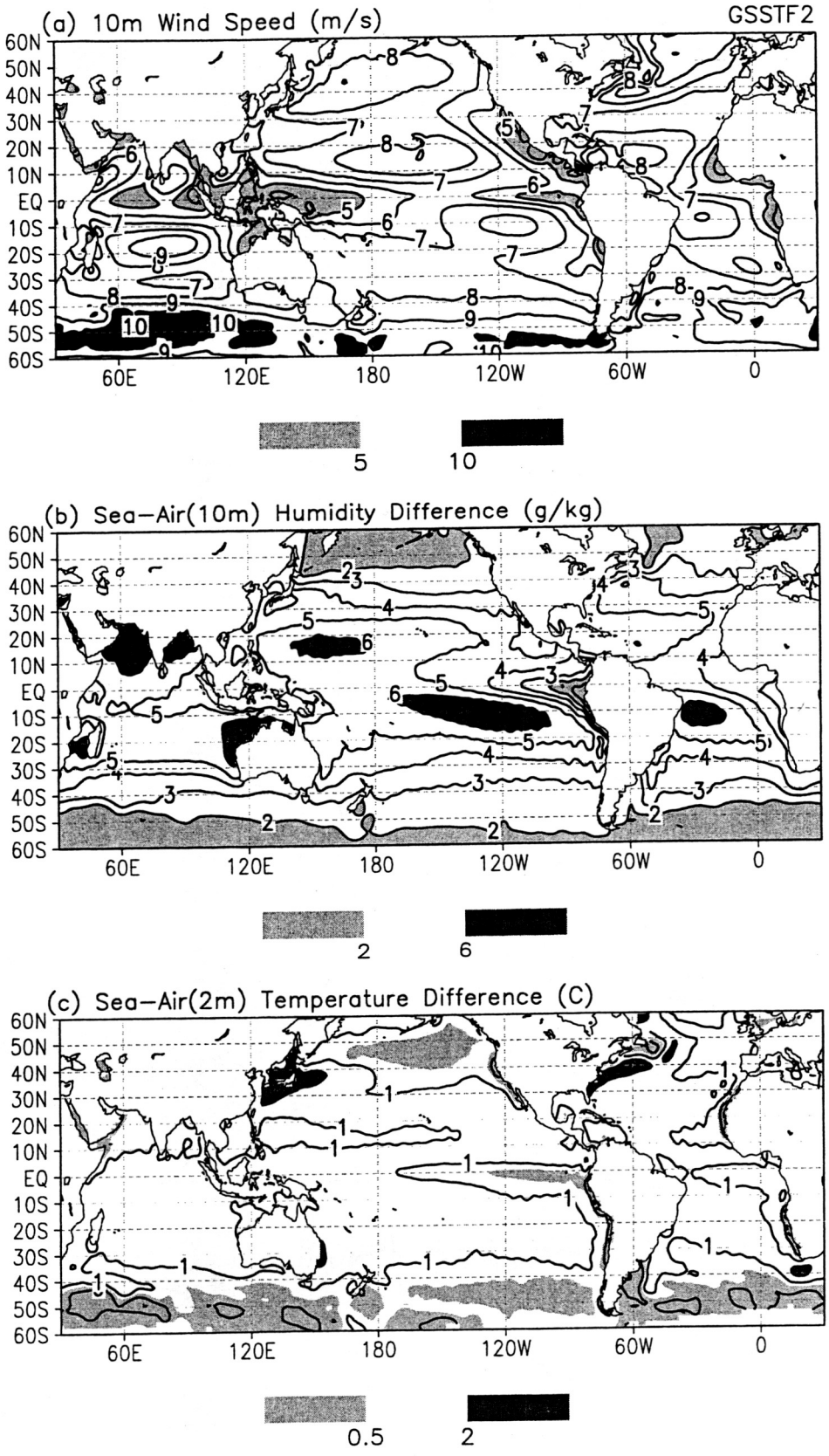
1988–2000 Annual Average
(a) 10m Wind Speed (m/s)
GSSTF2
60N
50N
40N
30N
20N
10N
EQ
10S
20S
30S
40S
50S
60S
60E
120E
180
120W
60W
0
5
10
(b) Sea–Air(10m) Humidity Difference (g/kg)
2
6
(c) Sea–Air(2m) Temperature Difference (C)
0.5
2

Fig. 3

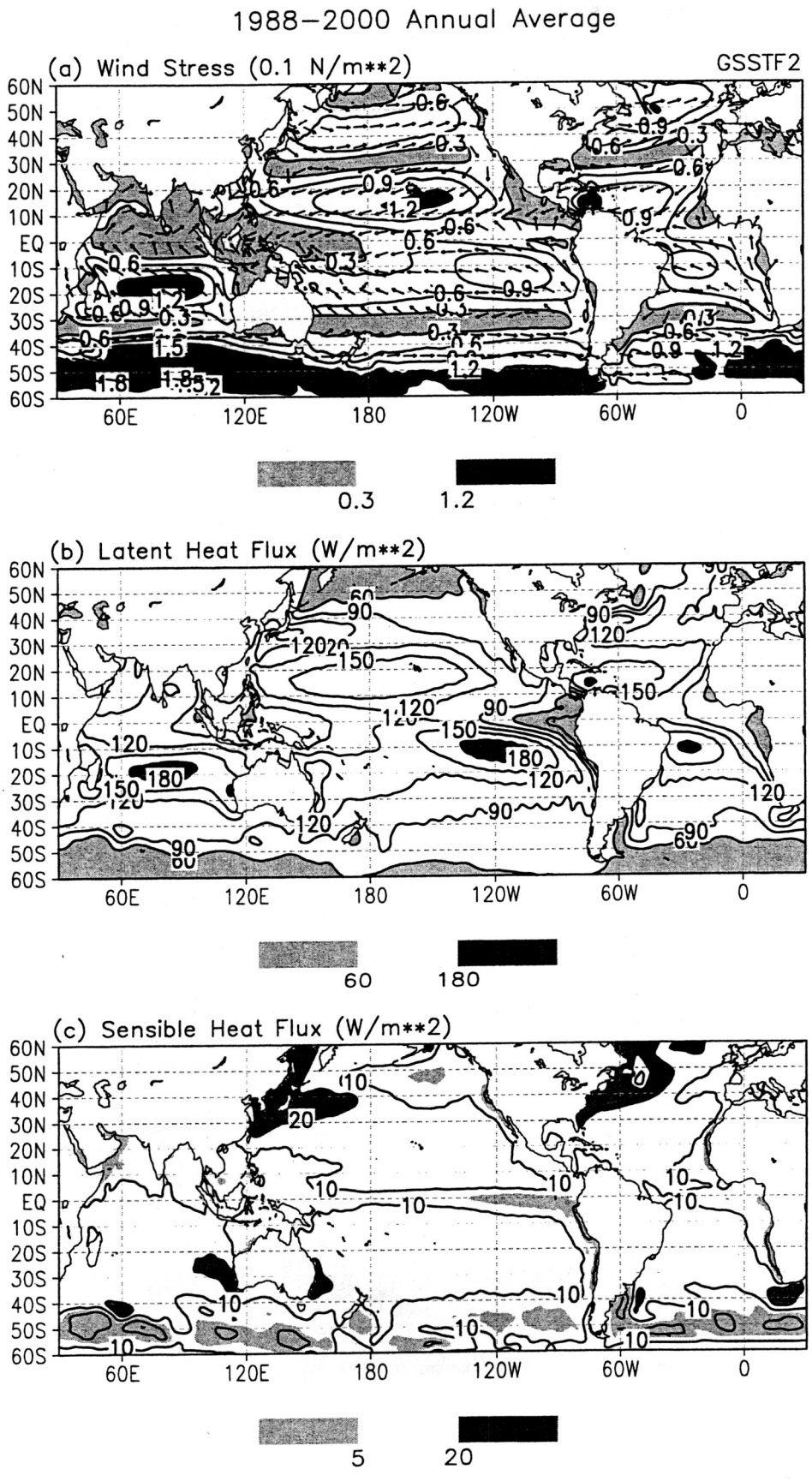
1988–2000 Annual Average
(a) Wind Stress (0.1 N/m**2)
GSSTF2
60N
50N
40N
30N
20N
10N
EQ
10S
20S
30S
40S
50S
60S
60E
120E
180
120W
60W
0
0.3
1.2
(b) Latent Heat Flux (W/m**2)
60
180
(c) Sensible Heat Flux (W/m**2)
5
20

Fig. 4

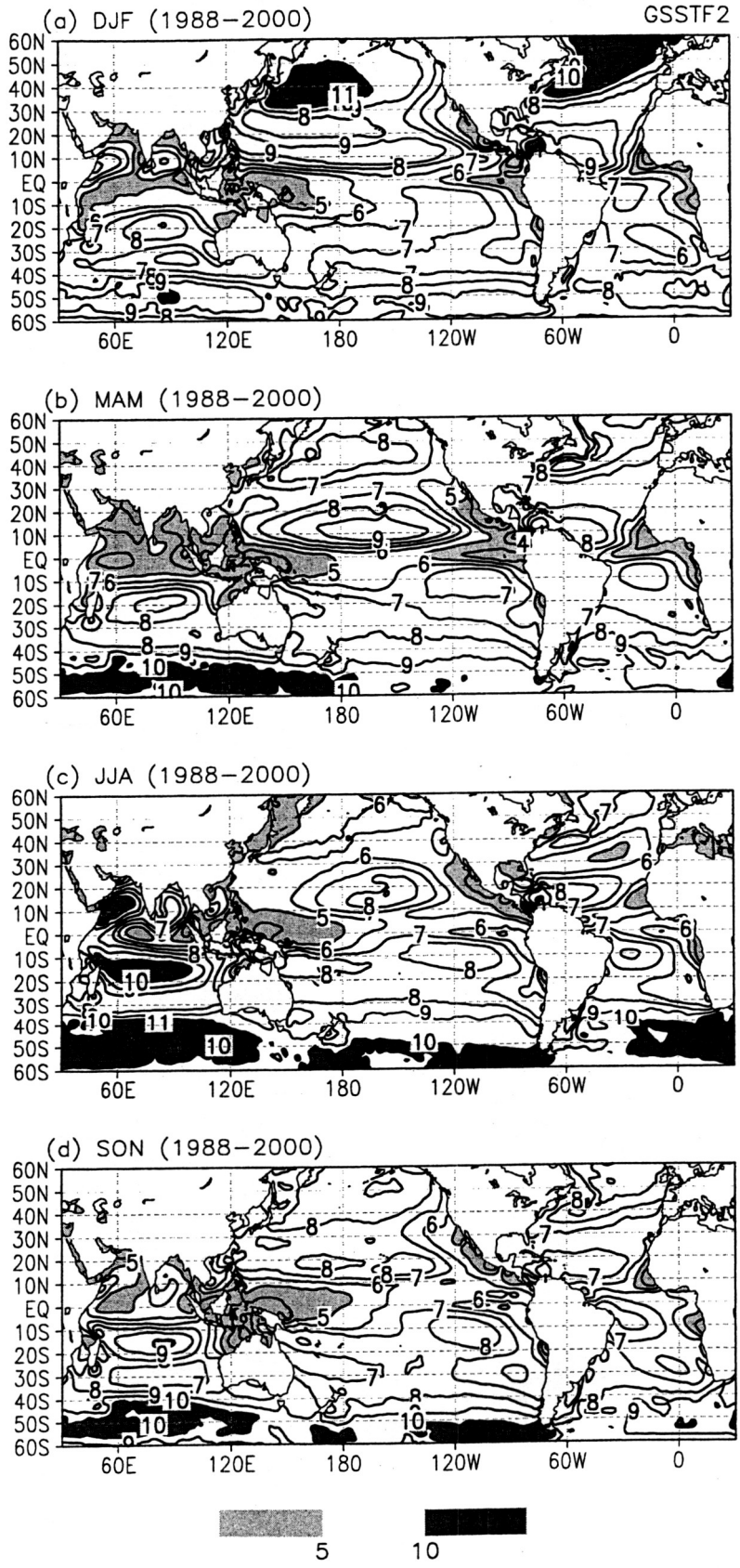
Seasonal Mean 10m Wind Speed (m/s)
(a) DJF (1988–2000)
GSSTF2
(b) MAM (1988–2000)
(c) JJA (1988–2000)
(d) SON (1988–2000)
60N
50N
40N
30N
20N
10N
EQ
10S
20S
30S
40S
50S
60S
60E
120E
180
120W
60W
0
5
10

Fig. 5

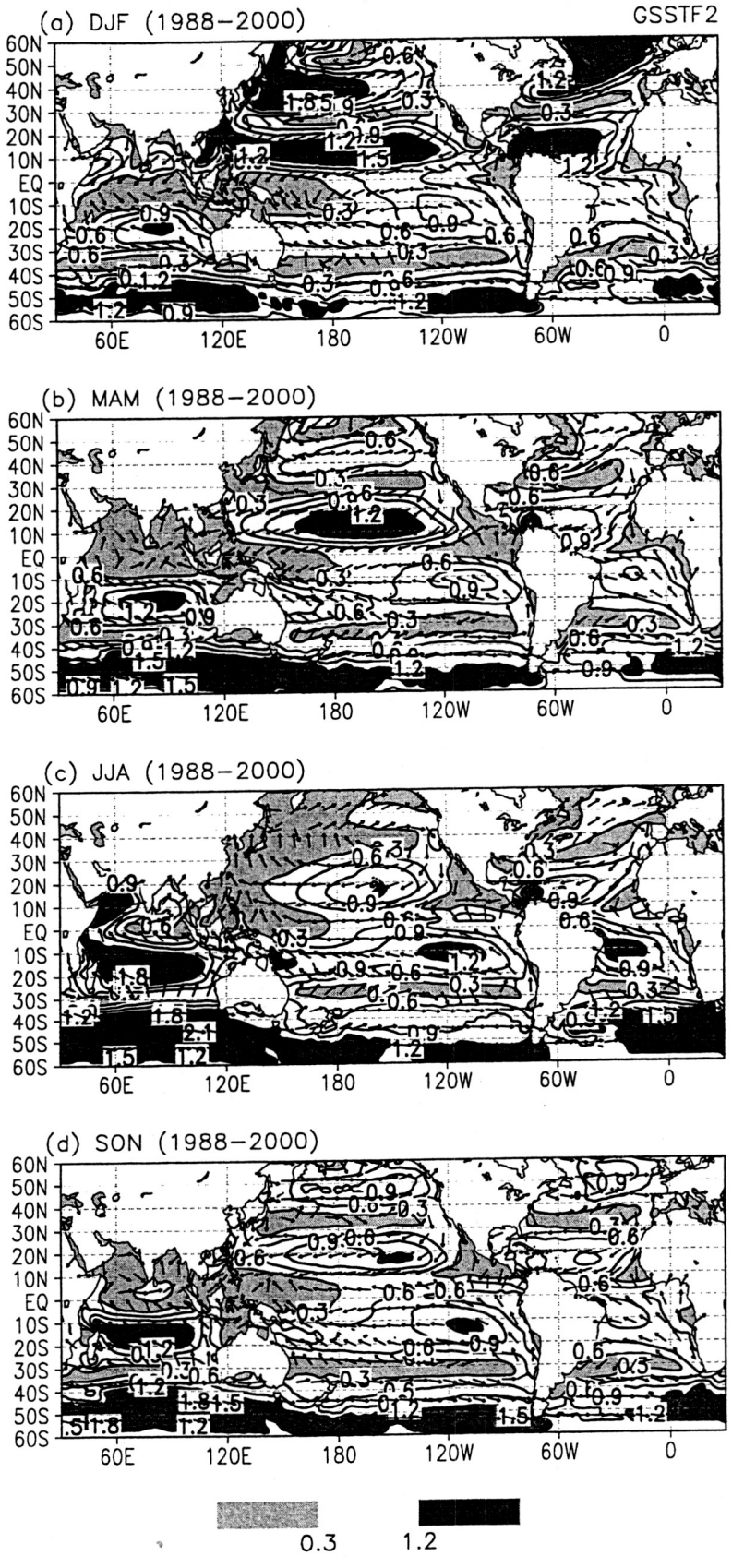
Seasonal Mean Wind Stress (0.1 N/m**2)
(a) DJF (1988–2000)
GSSTF2
(b) MAM (1988–2000)
(c) JJA (1988–2000)
(d) SON (1988–2000)
60N
50N
40N
30N
20N
10N
EQ
10S
20S
30S
40S
50S
60S
60E
120E
180
120W
60W
0
0.3
1.2

Fig. 6

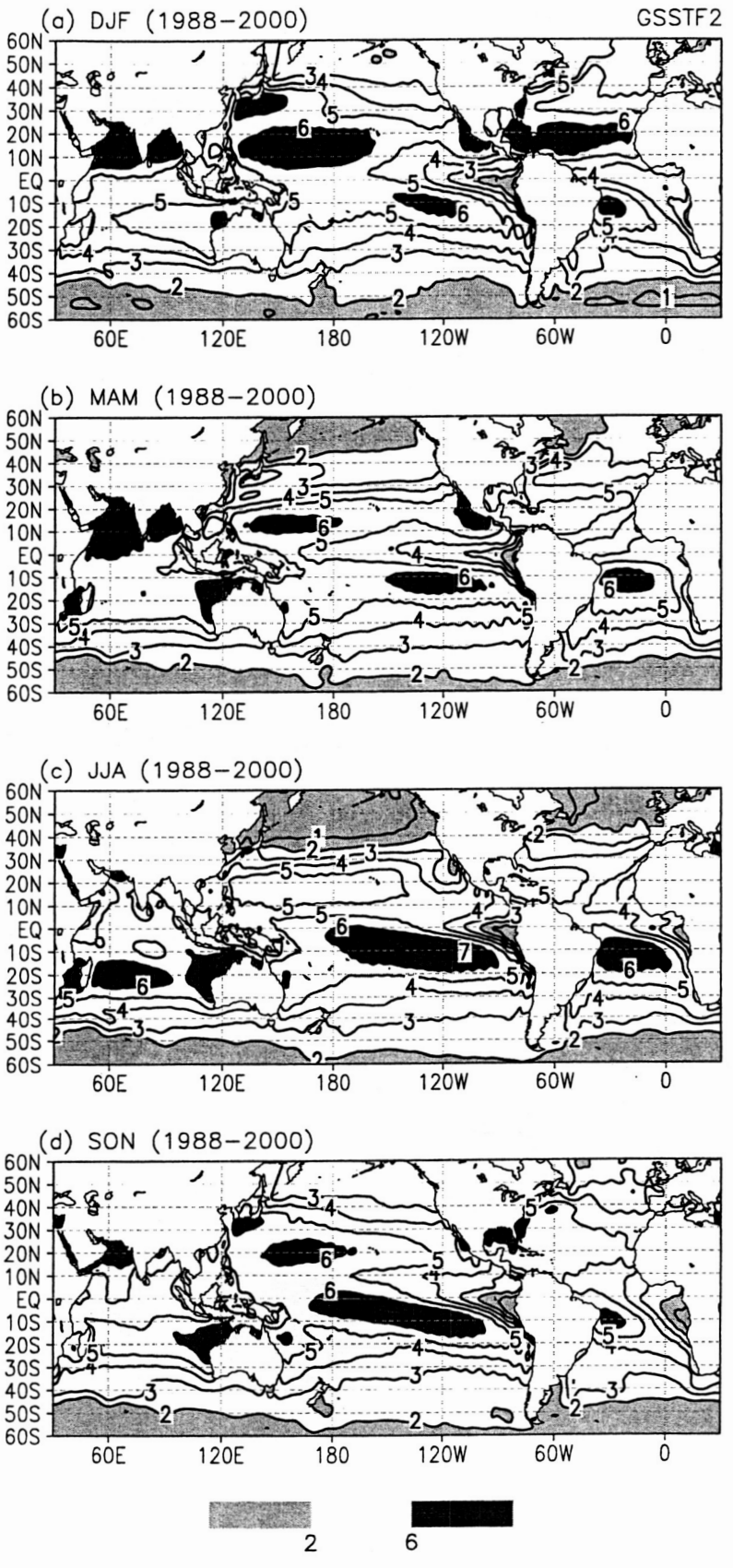
Seasonal Mean Sea−Air(10m) Humidity Difference (g/kg)
(a) DJF (1988−2000)
GSSTF2
(b) MAM (1988−2000)
(c) JJA (1988−2000)
(d) SON (1988−2000)
60N
50N
40N
30N
20N
10N
EQ
10S
20S
30S
40S
50S
60S
60E
120E
180
120W
60W
0
2
6

Fig. 7

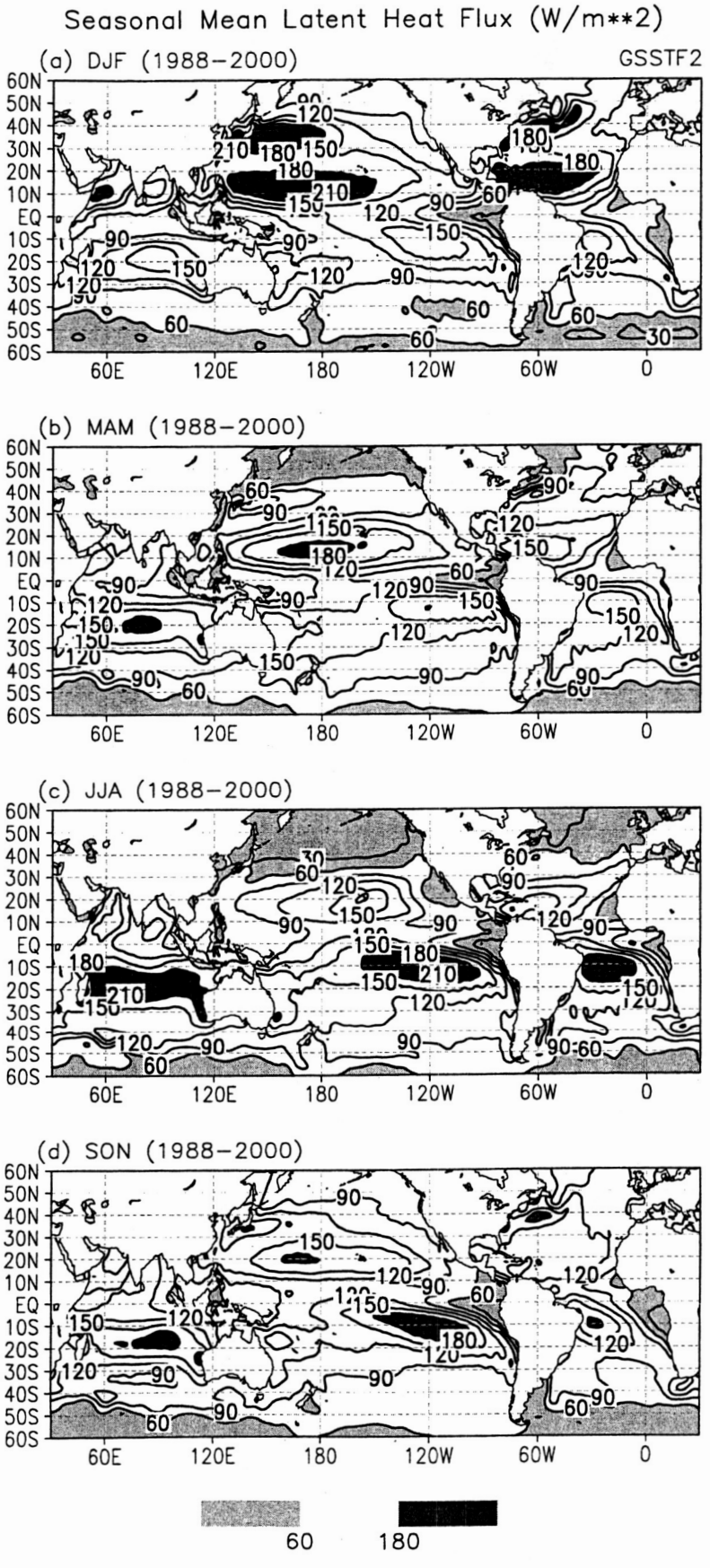
Seasonal Mean Latent Heat Flux (W/m**2)
(a) DJF (1988–2000)
GSSTF2
(b) MAM (1988–2000)
(c) JJA (1988–2000)
(d) SON (1988–2000)
60N
50N
40N
30N
20N
10N
EQ
10S
20S
30S
40S
50S
60S
60E
120E
180
120W
60W
0
60
180

Fig. 8

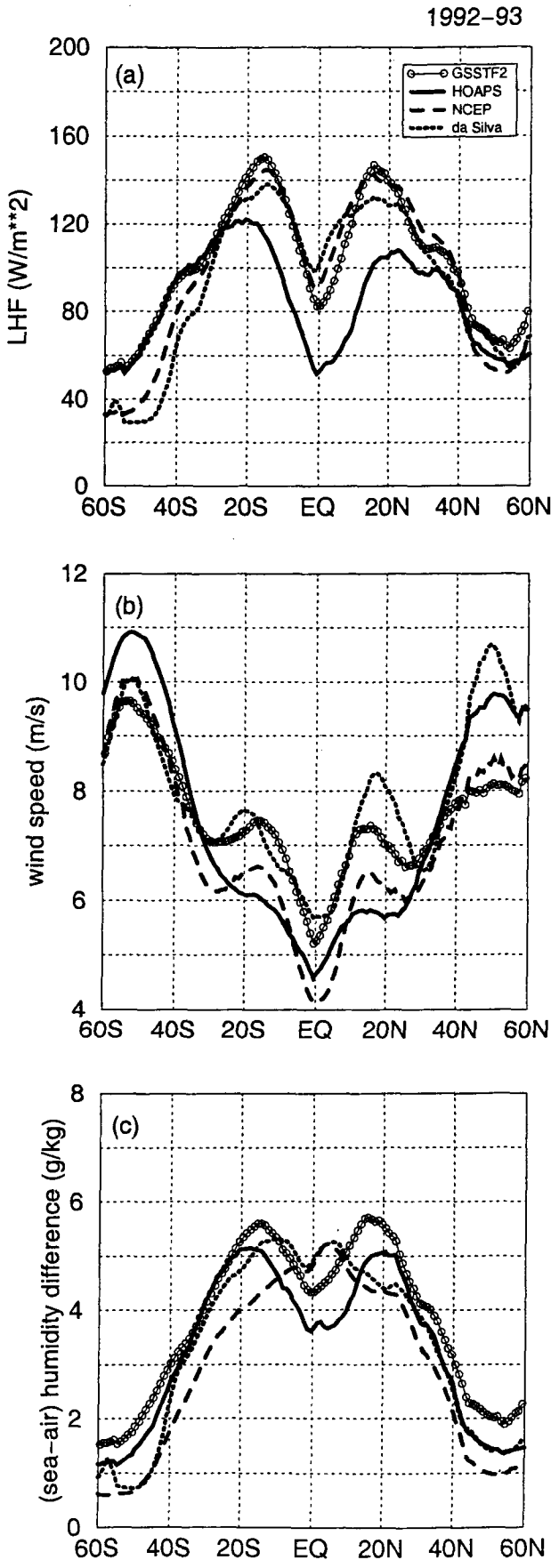
1992-93
(a)
GSSTF2
HOAPS
NCEP
da Silva
LHF (W/m**2)
200
160
120
80
40
0
60S
40S
20S
EQ
20N
40N
60N
(b)
wind speed (m/s)
12
10
8
6
4
(c)
(sea-air) humidity difference (g/kg)
8
6
4
2
0

Fig. 9

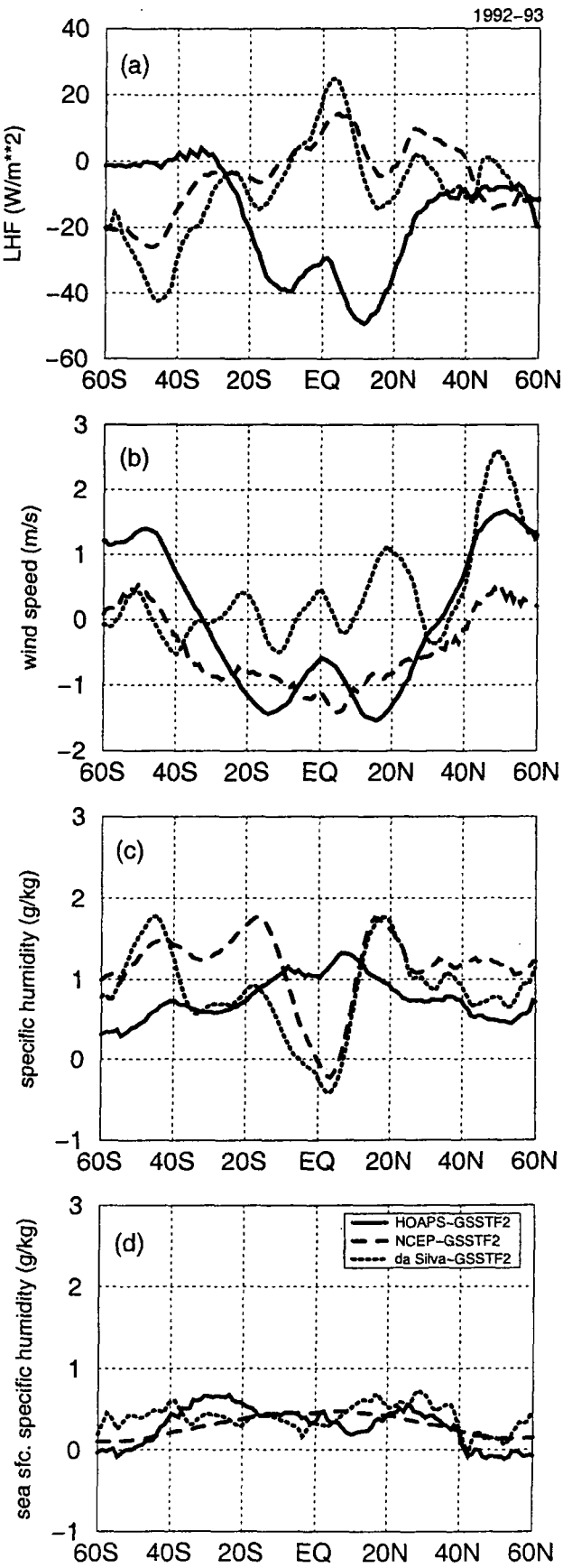
1992-93
(a)
LHF (W/m**2)
40
20
0
-20
-40
-60
60S 40S 20S EQ 20N 40N 60N
(b)
wind speed (m/s)
3
2
1
0
-1
-2
60S 40S 20S EQ 20N 40N 60N
(c)
specific humidity (g/kg)
3
2
1
0
-1
60S 40S 20S EQ 20N 40N 60N
(d)
sea sfc. specific humidity (g/kg)
HOAPS-GSSTF2
NCEP-GSSTF2
da Silva-GSSTF2
3
2
1
0
-1
60S 40S 20S EQ 20N 40N 60N

Fig. 10

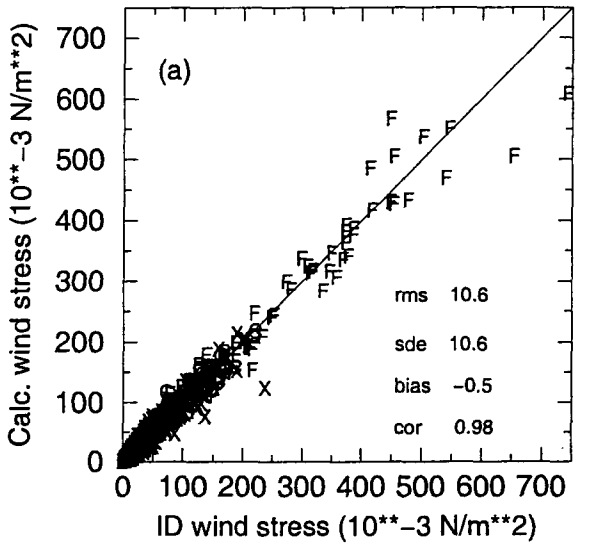
(a)
Calc. wind stress (10**−3 N/m**2)
ID wind stress (10**−3 N/m**2)
rms 10.6
sde 10.6
bias −0.5
cor 0.98
0
100
200
300
400
500
600
700

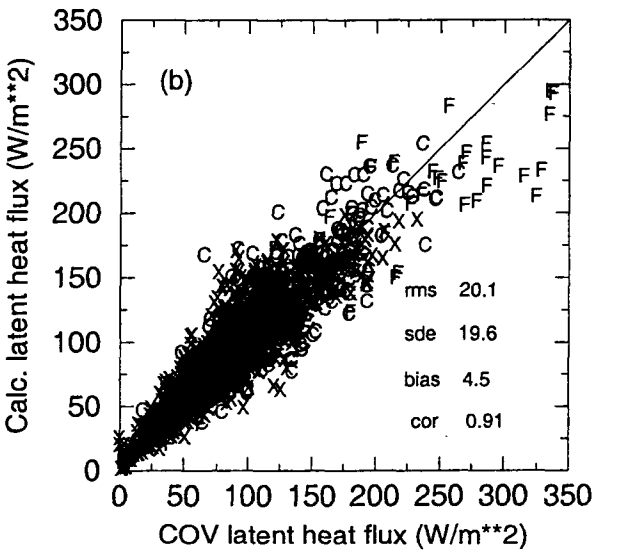
(b)
Calc. latent heat flux (W/m**2)
COV latent heat flux (W/m**2)
rms 20.1
sde 19.6
bias 4.5
cor 0.91
0
50
100
150
200
250
300
350

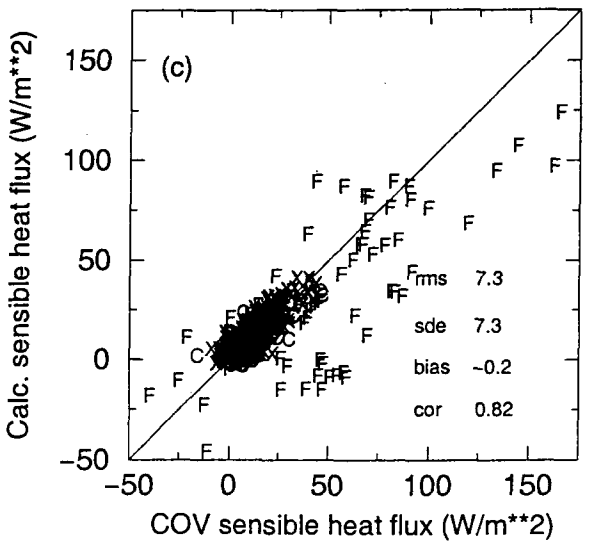
(c)
Calc. sensible heat flux (W/m**2)
COV sensible heat flux (W/m**2)
rms 7.3
sde 7.3
bias −0.2
cor 0.82
−50
0
50
100
150

Fig. A1

VERSION 2 GODDARD SATELLITE-BASED SURFACE TURBULENT FLUXES (GSSTF2)

Shu-Hsien Chou, Eric Nelkin, Joe Ardizzone, Robert M. Atlas, and Chung-Lin Shie

Popular Summary

Information on the turbulent fluxes of momentum, moisture, and heat at the air-sea interface is essential in improving model simulations of climate variations and in climate studies. We have derived a 13.5-year (July 1987–December 2000) dataset of daily surface turbulent fluxes over global oceans from the Special Sensor Microwave/Imager (SSM/I) radiance measurements. This dataset, version 2 Goddard Satellite-based Surface Turbulent Fluxes (GSSTF2), has a spatial resolution of 1° x 1° latitude-longitude and a temporal resolution of 1 day. Turbulent fluxes are derived from the SSM/I surface winds and surface air humidity, as well as the 2-m air and sea surface temperatures (SST) of the NCEP/NCAR reanalysis, using a bulk aerodynamic algorithm based on the surface layer similarity theory.

Hourly fluxes computed from the GSSTF2 bulk aerodynamic algorithm using the observed hourly input parameters agree well with those derived from ship observations of ten field experiments over the tropical and midlatitude oceans during 1991–99. In addition, the GSSTF2 daily wind stress, latent heat flux, wind speed, surface air humidity and SST compare reasonably well with those of the collocated ship measurements. The global distributions of 1988–2000 annual- and seasonal-mean turbulent fluxes show reasonable patterns related to the atmospheric general circulation and seasonal variations. Zonal averages of latent heat fluxes and input parameters over global oceans during 1992–93 have been compared among GSSTF1 (version 1), GSSTF2, HOAPS (Hamburg Ocean Atmosphere Parameters and Fluxes from Satellite Data), NCEP/NCAR reanalysis, and one based on COADS (Comprehensive Ocean-Atmosphere Data Set). Significant differences are found among these five flux datasets. Our analyses suggest that the GSSTF2 latent heat flux, surface air humidity, and winds are likely to be more realistic than the other four flux datasets examined, although those of GSSTF2 are still subject to regional biases. The GSSTF2 is useful for climate studies and is available at http://daac.gsfc.nasa.gov/CAMPAIGN_DOCS/hydrology/hd_gsstf2.0.html. This dataset has been submitted to the SEAFLUX Project, an ocean surface turbulent flux project, for intercomparison studies.